HHS Public Access

Author manuscript

Int J Radiat Oncol Biol Phys. Author manuscript; available in PMC 2021 August 03.

Published in final edited form as:

Int J Radiat Oncol Biol Phys. 2021 March 15; 109(4): 1040–1053. doi:10.1016/j.ijrobp.2020.10.025.

Melanoma cell intrinsic $GABA_A$ receptor enhancement potentiates radiation and immune checkpoint inhibitor response by promoting direct and T cell-mediated anti-tumor activity

Daniel A. Pomeranz Krummel, PhD[1,‡], **Tahseen H. Nasti, PhD**[2,‡], **Milota Kaluzova, PhD**[3], **Laura Kallay, PhD**[1], **Debanjan Bhattacharya, PhD**[1], **Johannes C. Melms, MD**[4], **Benjamin Izar, MD, PhD**[4], **Maxwell Xu, BS**[5], **Andre Burnham, PhD**[3], **Taukir Ahmed, PhD**[6], **Guanguan Li, PhD**[6], **David Lawson, MD**[7], **Jeanne Kowalski, PhD**[8], **Yichun Cao, MPH**[9], **Jeffrey M. Switchenko, Ph.D.**[9,10], **Dan Ionascu, PhD**[11], **James M. Cook, PhD**[6], **Mario Medvedovic, PhD**[12], **Andrew Jenkins, PhD**[13], **Mohammad K. Khan, MD, PhD**[14], **Soma Sengupta, MD, PhD**[1]

[1]Department of Neurology & Rehabilitation Medicine, University of Cincinnati College of Medicine, Cincinnati, OH, USA.

[2]Department of Microbiology & Immunology, Emory Univ. School of Medicine, Atlanta, GA, USA.

[3]Emory Univ. School of Medicine, Atlanta, GA, USA.

[4]Columbia Center for Translational Immunology, Columbia University College of Physicians and Surgeons, New York, NY, USA.

[5]Johns Hopkins University, Baltimore, MD, USA.

[6]Department of Chemistry & Biochemistry, Univ. of Wisconsin-Milwaukee, Milwaukee, WI, USA.

[7]Department of Hematology & Medical Oncology, Winship Cancer Institute of Emory University, Atlanta, GA, USA.

[8]Department of Oncology, LIVESTRONG Cancer Institutes, Dell Medical School, Univ. of Texas, Austin, TX, USA.

[9]Biostatistics Shared Resource, Winship Cancer Institute of Emory University, Atlanta, GA, USA.

[10]Department of Biostatistics & Bioinformatics, Rollins School of Public Health, Emory University, Atlanta, GA, USA.

[11]Department of Radiation Oncology, University of Cincinnati College of Medicine, Cincinnati, OH, USA.

[12]Department of Environmental Health, University of Cincinnati College of Medicine, Cincinnati, OH, USA.

Corresponding authors: Soma Sengupta, University of Cincinnati College of Medicine, The Vontz Center for Molecular Studies, ML: 0521; 3125 Eden Avenue, Cincinnati, OH, USA 45267; sengupsm@ucmail.uc.edu; Phone: (513) 558-0119, Mohammad K. Khan, Emory University School of Medicine, 1365C Clifton Rd., Atlanta, GA, USA 30322; drkhurram2000@gmail.com; Phone: (404) 778-5000.

Author of Statistical Analysis: Mario Medvedovic, University of Cincinnati College of Medicine, Kettering Laboratory, 160 Panzeca Way, Cincinnati, OH, USA 45267; medvedm@ucmail.uc.edu; Phone: (513) 281-2513

‡Co-first authors

[13]Departments of Anesthesiology, Pharmacology & Chemical Biology, Emory Univ. School of Medicine, Atlanta, GA, USA.

[14]Department of Radiation Oncology, Winship Cancer Institute of Emory University, Atlanta, GA, USA.

Abstract

Purpose: Most metastatic melanoma patients show variable responses to radiotherapy and do not benefit from immune checkpoint inhibitors (ICIs). Improved strategies for combination therapy that leverage potential benefits from radiotherapy and ICI are critical.

Methods and Materials: We analyzed metastatic melanoma tumors in the TCGA cohort for expression of genes coding for subunits of Type-A γ-aminobutyric acid (GABA) receptor ($GABA_AR$), a chloride ion channel and major inhibitory neurotransmitter receptor. Electrophysiology was used to determine if melanoma cells possess intrinsic $GABA_AR$ activity. Melanoma cell viability studies were conducted to test if enhancing $GABA_AR$ mediated chloride transport using a benzodiazepine impaired viability. While a syngeneic melanoma mouse model was used to assay the effect of benzodiazepine on tumor volume and its ability to potentiate radiation and/or immunotherapy. Treated tumors were analyzed for changes in gene expression by RNA sequencing and presence of tumor infilitrating lymphocytes by flow cytometry.

Results: Genes coding for subunits of $GABA_ARs$ express functional $GABA_ARs$ in melanoma cells. By enhancing $GABA_AR$ mediated anion transport, benzodiazepines depolarize melanoma cells and impair their viability. *In vivo*, benzodiazepine alone reduces tumor growth and potentiates radiotherapy and α-PD-L1 anti-tumor activity. Combination of benzodiazepine, radiotherapy, and α-PD-L1 results in near complete regression of treated tumors and a potent abscopal effect, mediated by increased infiltration of polyfunctional CD8+ T cells. Treated tumors show expression of cytokine:cytokine receptor interactions and overrepresentation of p53 signaling.

Conclusions: This study identifies an anti-tumor strategy combining radiation and/or immune checkpoint inhibitor with modulation of $GABA_ARs$ in melanoma using a benzodiazepine.

Introduction

Incidence of melanoma continues to rise and advanced disease confers a poor prognosis.[1] Approximately 50% of melanomas harbor somatic B-raf (*BRAF*) mutations[2, 3], which sensitizes them to treatment with BRAF or BRAF/MEK inhibitor combinations. First generation of a clinically active BRAF-inhibitor produced high systemic objective response rates.[4] Subsequent development of next-generation combination therapies with BRAF/MEK-inhibitors, further improved progression-free survival.[5–7] However, the majority of patients acquire resistance to these therapies.[8—11] More recently, a combination of immune checkpoint inhibitors targeting programmed cell death-1 (PD-1) and cytotoxic T-lymphocyte-associated protein 4 (CTLA-4) produced an overall response rate of ~60% and durable responses in a portion of patients, including those with melanoma brain metastases.[12–16] However, the majority of metastatic melanoma patients do not experience durable responses.

While significant progress has been made, novel therapeutic strategies to treat BRAF/MEK inhibitor or ICI resistant disease are desperately needed. Furthermore, there are unique clinical challenges, such as presence of melanoma brain metastases, which are associated with significant morbidity and mortality, and the brain may represent a therapeutic sanctuary site because of the blood-brain barrier.

Gene expression analysis by The Cancer Genome Atlas (TCGA) of melanoma patient tumors revealed that *GABR* genes, which code for subunits of the Type-A γ-aminobutyric acid (GABA) neurotransmitter receptor ($GABA_AR$), are amongst those most highly expressed.[17] We conducted a more extensive analysis of *GABR* expression in metastatic melanoma tumors as well as characterization of melanoma cells for intrinsic $GABA_AR$ activity. We find that melanoma patient expression of *GABR* genes varied with the molecular subgroups of melanoma defined by TCGA, including MITF-low and Keratin groups, and that melanoma cells express functional $GABA_ARs$. Furthermore, enhanced $GABA_AR$ mediated membrane permeability to anions with $GABA_AR$ subtype-preferring benzodiazepines, results in depolarized mitochondria in melanoma cells and impaired cell viability. In a syngeneic melanoma mouse model, benzodiazepine alone reduces tumor growth and when combined with radiation and/or α-PD-L1, potentiated effectiveness. Benzodiazepine with radiation promotes both ipsilateral and an abscopal anti-tumor activity associated with increased tumor infiltration with antigen-specific polyfunctional CD8 T-cells. Our study identifies a potential novel anti-tumor strategy combining radiation and/or immune checkpoint inhibitor with modulation of $GABA_ARs$ in melanoma using a benzodiazepine.

Methods and Materials

Cell lines.

Cell lines were purchased from American Type Culture Collection (ATCC). B16F10 was transduced with lentiviral vector expressing Lymphocytic choriomeningitis Glycoprotein (GP).

Electrophysiology.

Intracellular saline solution contained: 145 mM CsCl, 2 mM $CaCl_2$, 2 mM $MgCl_2$, 10 mM EGTA, 10 mM HEPES. Extracellular saline solution contained: 140 mM NaCl, 5 mM KCl, 2 mM $CaCl_2$, 1 mM $MgCl_2$, 10 mM HEPES, 10 mM D-glucose. Both were adjusted to pH 7.4 (320–330 mOsm) and 0.2 μm filter sterilized. A375 and B16F10-GP cells were dissociated with detachin (Genlantis), suspended in extracellular saline (2.5×10^6 cells/mL), and agitated prior to loading into 384-well fluxion ensemble plates. Cells were patched using an Ionflux Mercury microfluidic automated patch clamp system (Fluxion Biosciences). Up to 1,280 cells were patched at −60 mV using an automated suction protocol, followed by superfusion with ligand and drug combinations. Current data was recorded (10 kHz) for offline analysis with bespoke MatLab scripts.

Cell viability.

Benzodiazepines, synthesized as described[19], were suspended in dimethyl sulfoxide (DMSO; 0.125%) and added to plated cells. After 24 or 48 hour incubation of benzodiazepine or DMSO vehicle control (37°C, 5% CO_2), 20 μL CellTiter 96® AQueous One Solution (Promega) was added per well, plate incubated 1 hour (37°C), and absorbance (490 nm) measured. To calculate % cell viability, media control (average reading of wells containing only media) was subtracted from DMSO control and drug-treated values. Drug-treated values were normalized by dividing by mean DMSO absorbance values and converting to percent. IC_{50} values were obtained using GraphPad Prism7 (GraphPad).

Mouse experiments.

B16F10-GP cells (5×10^5) were implanted in matrigel (25%) on right/left-flanks of 6–8 week old female C57BL/6 mice (Jackson Laboratories). Palpable tumors (10 days) were irradiated right-side with a Superflab bolus (0.5 cm tissue equivalent material) placed over tumor and thereafter tumor measurements taken as indicated. The Superflab bolus allows for a maximum surface to the tumor and reduces penetration of the rays to the internal body organs Irradiation was done using an X-RAD 320 irradiation unit, a self-contained X-ray system for delivering a precise radiation dosage. The shielded cabinet includes an Adjustable Specimen Shelf, Sample Viewing Window and Beam Hardening Filter Holder. The 320-kV/10mA X-ray tube provides a high output with a uniform vertical beam and maximum output of 4000 W permitting delivery of up to 15 Gy/min at 50-cm source to surface distance. The actual dose and rate and amount of energy produced depends on other factors, including beam filtration and other exposure settings. To avoid scatter, a light beam of 3 mm^2 was focused on the tumor (right flank only) and mice were irradiated (5 or 10 Gy) while under anesthesia. Tumor diameters were measured using calipers and volume calculated using the formula for an ellipse (i.e. $4/3\pi$.(l.w.h), where l, w, h are three radii of the tumor taken perpendicullar to each other). Mice were used in accordance with Institutional Animal Care and Use Committee.

Tumor infilitrating lymphocytes (TILs) isolation and flow cytometry.

Tumors were harvested, minced, digested with collagenase IV (150 U/mL) and DNAse (20 μg/mL), centrifuged, and suspended in 5% RPMI. Suspension was layered on top of histopaque (Sigma), TILs collected at the interface, stained, run on LSRII (BD) or BD FACSCanto, and analyzed (FlowJo software). For intracellular cytokine analysis, TILs were isolated from tumor and stimulated (6 hours) in presence of brefeldin and myostatin with LCMV specific glycoprotein peptide GP33–41, stained with antibodies of interest, and analyzed by flow.

RNA-seq and data analysis.

RNA extracted from tumors met the following requirements: ≥750 ng RNA, a preferred concentration 10 ng/μL, DV200>0.3 (where DC200 is fraction of RNA fragments whose length is >200 nucleotides). RNA was processed and sequenced at the Broad Institute by the Transcriptome Capture method using Illumina HiSeq2500. Sequence reads were aligned to reference mouse genome (mm10) using STAR aligner[20] and reads aligning to each known

gene were counted using featureCounts.[21] Differential expression analysis between different samples was performed based on the negative-binomial statistical model of read counts as implemented in the edgeR Bioconductor package[22] and *p*-values adjusted using False Discovery Rates.[23] Enrichment KEGG pathways[24], transcription factor targets[25], and ImmuneSigDB gene sets[26] were identified using gene set enrichment analysis[27] as implemented in the FGSEA R package[28] with 100,000 random permutations. Results were visualized using the ComplexHeatmap package.[29]

Results

$GABA_AR$ subunit expression in metastatic melanoma patient tumors.

Type A γ-aminobutyric acid (GABA) receptors ($GABA_ARs$) form pentameric chloride channels, composed most commonly of two α, two β, and γ subunits encoded by *GABR* genes *GABRA* (1–6), *GABRB* (1–3), and *GABRG* (1–3), respectively[30, 31] (Fig. 1a). We conducted a differential expression analysis of normal human melanocytes and metastatic melanoma patient-derived lines (Fig. E1). This analysis highlights a difference in expression between melanocytes and melanoma cells. Specifically, there is a significantly enhanced expression in the melanoma lines, relative to primary melanocyte lines, of *GABRA3*, *GABRA5* and *GABRA6* (FDR<0.1). We also conducted a comprehensive analysis of *GABR* expression in stage III/IV melanoma patients in the TCGA dataset of cutaneous melanoma[17] (Fig. 1b). This analysis reveals that in the 'MITF-low' subgroup patients, there is notable expression of *GABRA3, GABRB1,* and *GABRG2.* In contrast, 'Keratin' subgroup patients exhibit a greater enhanced expression of *GABRA5, GABRB3,* and *GABRG3.* 'Immune' subgroup patients similarly exhibit *GABR* expression, but not of a clear subset of *GABR* genes. A pairwise correlation analysis of the *GABR* expression patient data in the three TCGA proposed melanoma subgroups suggests there is correlated expression in MITF-low and Keratin subgroups that may yield $GABA_ARs$ composed of α3β1γ2 and α5β3γ3, respectively (Fig. E2).

To confirm expression of *GABR* genes in melanoma cells, we performed RT-PCR analysis for *GABR* expression in patient derived melanoma cell lines (A375, RPMI-7951, SKMEL-24, SKMEL-28). All lines express to a varying degree *GABRA3*, while SKMEL-24 and SKMEL-28 have uniquely high *GABRA2* and *GABRA5* expression, respectively (Fig. E3a and E3b). There is significantly less expression of *GABRB1–3* and *GABRG1–3* in these lines, compared to *GABRA1–6* levels. Western blotting of human melanoma line A375 and murine line B16F10-GP for subunits α2, α3 and α5 protein abundance is concordant with RT-PCR results (Fig. E3c).

Melanoma cells possess functional $GABA_ARs$.

$GABA_AR$ is a chloride channel that changes the transmembrane potential of cells, either depolarizing or hyperpolarizing depending upon the activity of other membrane transport proteins.[30, 31] To validate that expression of $GABA_AR$ subunits in melanoma cell lines leads to assembly of a functional receptor, we patch-clamped human (A375) and murine (B16F10-GP) melanoma lines to detect electrophysiological currents. Both lines exhibit a response to the neurotransmitter GABA, the $GABA_AR$ endogenous ligand (Fig. 2a; Table E1).

Compared to A375, B16F10-GP cells exhibited a larger maximal response to and a greater affinity for GABA.

Benzodiazepines bind at the α-γ interface of a $GABA_AR$ (Fig. 1a). A functional benzodiazepine binding site requires assembly of a $GABA_AR$ with a canonical αβαβγ subunit stoichiometry.[32, 33] Benzodiazepine binding increases the probability of the channel opening in the presence of GABA, thus increasing the flow of anions crossing the membrane. Since benzodiazepines interact with the $GABA_AR$ at a site different than GABA, we tested the effect of benzodiazepines on the current of A375 and B16F10-GP cells. We tested two benzodiazepines (QH-II-066 and KRM-II-08) to observe if an enhanced current was elicited. QH-II-066 and KRM-II-08 possess the privileged structure of diazepam, but with less sedative and ataxic effects than diazepam (valium) and chlordiazepoxide (librium).[19] This was achieved by a subtle alteration of their chemical structure (Fig. 1a) that increased preference for specific $GABA_AR$ subtypes, as opposed to diazepam. We find that QH-II-066 and KRM-II-08 enhance the effect of GABA (membrane anion permeability) in a dose-dependent manner in A375 and B16F10-GP cells (Fig. 2c and 2d; Table E1).

Benzodiazepine depolarizes melanoma cell membrane potential and impairs viability.

In our studies of the effect of benzodiazepine on medulloblastoma cells we showed that changes that followed the benzodiazepine mediated increase in membrane anion permeability included, depolarization of the mitochondrial transmembrane potential[18], ultimately resulting in apoptosis via the intrinsic mitochondria-mediated pathway. Thus, we tested if benzodiazepine elicited a similar response in A375 and B16F10-GP cells. To test if the melanoma cell membrane potential was changed, we used the cationic stain tetramethylrhodamine ethyl ether (TMRE) and fluorescence microscopy imaging of live cells. TMRE is taken-up by functioning mitochondria and exhibits reduced staining if the mitochondrial transmembrane is depolarized. At 10 minutes after exposure to QH-II-066, mitochondrial membranes of A375 and B16F10-GP cells are depolarized (Fig. E4), consistent with a flow of chloride anions out of the melanoma cell.

We examined if these benzodiazepines as well as diazepam impacted the viability of melanoma cells by treating A375 and B16F10-GP cells with QH-II-066, KRM-II-08, or diazepam over 48 hours. We observed a dose-dependent reduction in cell viability in both lines with QH-II-066 or KRM-II-08 (Fig. 2e and 2f). In contrast, diazepam had no effect on the viability of either A375 or B16F10-GP cells (Fig. E5a). Similar IC_{50} values were obtained for additional human metastatic melanoma lines treated with QH-II-066 and KRM-II-08 (Table E2). Cell lines which appeared to show no response to the benzodiazepines were those where *TP53* was mutated, which is consistent with a role of p53 signaling in the response of cells to the benzodiazepines, as noted in our medulloblastoma studies.[18, 34, 35]

To determine whether the effect on cell survival was benzodiazepine-specific, we tested the effect of allopregnanolone on cell viability. Allopregnanolone is also a positive allosteric modulator of $GABA_AR$ like benzodiazepines, but a non-benzodiazepine neurosteroid that does not bind at the canonical high affinity benzodiazepine binding site located at the α-γ interface. Allopregnanolone does not impair the viability of A375 or B16F10-GP lines (Fig. E5b), suggesting that the effect on melanoma cell survival is benzodiazepine-specific or at

least specific to the more selective benzodiazepine-derivatives tested (QH-II-066 and KRM-II-088). In addition, we tested the effect of QH-II-066 on viability of a primary human melanocyte cell line (Fig. E6). At a concentration above the QH-II-066 IC_{50} for the human melanoma lines tested, there is no difference in melanocyte morphology as compared to the control indicating that QH-II-066 does not grossly impact normal, noncancerous melanocytes.

Benzodiazepine alone reduces tumor growth.

Since we observed that melanoma cell viability *in vitro* was impaired by benzodiazepines QH-II-066 and KRM-II-08 (albeit with a modest IC_{50}), we investigated if benzodiazepine had anti-tumor activity in the B16F10-GP syngeneic melanoma murine model. We used QH-II-066 for *in vivo* testing given that this compound has previously been tested in primates as an anxiolytic without any adverse effects or toxicity[36], while KRM-II-08 has not been similarly tested. In addition, QH-II-066 is more soluble, making it more experimentally tractable. We observed a dose-dependent reduction in B16F10-GP tumor growth at three QH-II-066 dosage points (10, 25, 50 mg/kg) (Fig. E7). There is negligible difference between doses 25 and 50 mg/kg, indicating that a lower dose of the benzodiazepine is sufficient for anti-tumor activity in an otherwise aggressive melanoma model. At the conclusion of the experiment we recorded the weight of mice to assess toxicity. The weights between mice were not significantly different (Fig. E8).

Benzodiazepine anti-tumor activity is potentiated in combination with either radiotherapy or α-PD-L1.

In our earlier study on medulloblastoma, we found that a benzodiazepine was capable of sensitizing cells in culture to radiation. We similarly evaluated the survival and proliferation of B16F10-GP cells following treatment with QH-II-066 ± radiation in culture using a clonogenic assay (Fig. E9). We find that QH-II-066 potentiates radiation and the combined treatment (QH-II-066+radiation) impacts survival and proliferation of B16F10-GP cells more significantly than either QH-II-066 or radiation alone. Based on the clonogenic assay result, we reasoned that a benzodiazepine might be beneficial in potentiating radiation in an *in vivo* model and that this should be explored in a model that is immunocompetent, given that varied immune cells may also possess $GABA_A$Rs and contribute in some manner to increase effectiveness of QH-II-066. We used the established B16F10-GP syngeneic melanoma murine model to assess whether QH-II-066 potentiates radiation to control both ipsilateral and contralateral tumor volume. Further, we chose to use a dose of 10 mg/kg QH-II-066, which by itself had little direct anti-tumor activity relative to the higher doses tested. Using this dose our objective was to clearly assess the impact of QH-II-066 in combination with radiation.

We implanted B16F10-GP melanoma cells in both right and left-flanks of C57BL/6 mice (Fig. 3a). A single dose of radiation (either 10 or 5 Gy) was delivered to the right-flank only on Day 10 after tumor implantation, when tumors are palpable. We find that combination of radiation plus QH-II-066 resulted in significantly reduced ipsilateral and contralateral tumor volume, when compared to either monotherapy (benzodiazepine or radiation alone) or the control (Fig. 3a; Fig. E10). A statistical analysis of tumor growth delay indicated by fraction

of tumors that doubled over time, shows a significant change in combination treatment groups (Fig. E11). These results indicated a possible synergistic anti-tumor response of benzodiazepine plus radiation and a potent out of field abscopal effect of this combination in an otherwise highly treatment resistant tumor model. The mice weights did not indicate any toxicity concerns due to radiation and or combination of the drug and radiation (Fig. E8).

We sequenced transcriptomes of the treated tumors. In comparison to the control, we identified: 42 differentially expressed (FDR<0.1) genes in QH-II-066 treated tumors; 1564 differentially expressed genes in the radiation treated tumors; and 587 differentially expressed genes in QH-II-066 plus radiation treated tumors. Enrichment analyses of gene expression for all Kyoto Encyclopedia of Genes and Genomes (KEGG) pathways and transcription factor targets revealed statistically significant up-regulation in all three treatment groups in comparison to control, of genes with roles in the cytokine:cytokine receptor interaction pathway, whereas target genes of p63, a member of the p53 family of transcription factors, were up-regulated in the radiation and QH-II-066 plus radiation treated tumors (Fig. 4; Fig. E12). Increased expression of *TP63* has been associated with the genotoxic treatment of melanoma cell lines[37], and in our results the enrichment of p63 targets was corroborated by the increased expression of *TP63* in the radiation and QH-II-066 plus radiation treated tumors (>100-fold increase, FDR<0.0002 in both comparisons), but not in the QH-II-066 alone treated tumors (FDR>0.7). We also conducted an enrichment analysis of the ImmuneSigDB compendium of transcriptional immune signatures. This analysis identified enhanced expression of genes associated with overexpression of microRNA mir-17, whose expression has also been shown to be enhanced by p63.[38]

Having observed that QH-II-066 could sensitize a melanoma tumor to radiation and that expression of genes with roles in the cytokine:cytokine receptor interaction pathway was enhanced, we examined if potentiation could be extended to an immune checkpoint inhibitor. Immune checkpoint inhibitors have shown some degree of success in treatment of metastatic melanoma, but most patients with advanced disease exhibit poor and variable response to immunotherapy.[12–16] We examined if QH-II-066 potentiated the anti-tumor response of programmed death ligand 1 immune checkpoint inhibitor (α-PD-L1) in B16F10-GP mice. Monotherapy treatment with QH-II-066 or α-PD-L1 resulted in comparable reductions in tumor volume. The most significant reduction in tumor volume is observed with QH-II-066 plus α-PD-L1 (Fig. 5; Fig. E11). Similar to what was observed for radiation, QH-II-066 and α-PD-L1 have a synergistic anti-tumor response.

Combined benzodiazepine, α-PD-L1, and radiotherapy results in significant tumor regression.

We reasoned that having observed potentiation of radiation and α-PD-L1 by QH-II-066 individually, there might be a more significant tumor response if a ‘combo’ consisting of radiation (5 Gy), α-PD-L1, plus QH-II-066 were administered.

Dual treatments of benzodiazepine plus radiation or benzodiazepine plus α-PD-L1 were better than radiation or α-PD-L1 alone (Fig. 6a), as reported above. Further, right-flank tumors which received radiation exhibited greater reduction in tumor growth in treatments including radiation, as expected based on above. There is again a pronounced abscopal effect

for non-irradiated left-flank tumors, as noted above. But clearly, the most significant ipsilateral and abscopal effect is seen in the combo treatment group, complete tumor regression in some animals (Fig. 6a). A similar observation is noted when tumor growth delay was calculated (Fig. E11). QH-II-066 plus radiation plus α-PD-L1 has a significant impact on tumor doubling time.

Immunophenotyping treated tumors.

To determine whether the apparent synergistic effect of benzodiazepine QH-II-066 plus radiation (10 or 5 Gy) and/or α-PD-L1 were mediated by an enhanced immune response, we performed immunophenotyping of bilateral tumors (Fig. 3b and 3c; Fig. 6b and 6c; Figs. E13–E15).

Compared to the control, QH-II-066 and radiation (5 or 10 Gy) monotherapies resulted in significantly increased numbers of tumor-infiltrating lymphocytes (TILs) in both ipsilateral and contralateral tumors. The dual therapy of QH-II-066 and radiation (5 or 10 Gy) results in a particularly pronounced increase in numbers of TILs in contralateral tumors, as compared to either radiation or QH-II-066 monotherapies. This effect appears most pronounced at the lower radiation dose (5 Gy) administered. Compared to the control, monotherapy and dual therapy, the combo therapy resulted in significantly increased numbers of TILs in both ipsilateral and contralateral tumors.

The total number of CD8+ T cells increased with radiation (10 or 5 Gy) in the ipsilateral tumor, as compared to the contralateral tumor (Fig. 3b; Fig. E13–15). When QH-II-066 is combined with radiation, there is a comparable increase in total number of CD8+ T cells in ipsilateral and contralateral tumors. While the number of CD8+ T cells increases in number in this treatment group, the overall portion of lymphocytes that are CD8+ T cells does not show a significant increase, indicating that QH-II-066 may elicit an infiltration of other immune cells into the tumor. While the total number of CD8+ T cells increased with radiation (10 or 5 Gy) alone and the dual combination of QH-II-066 plus radiation or α-PD-L1 in the ipsilateral tumor, GP33-antigen specific CD8+ cells significantly increased in both ipsilateral and contralateral tumors only in the dual or combo therapy groups, indicating a potent tumor-specific immune response.

Examination of the polyfunctionality of the CD8+ T cells reveals that the frequency of interferon-γ (IFN-γ) and IFN-γ/tumor necrosis factor-α (IFN-γ/TNF-α) producing CD8+ T cells were most significantly increased in both ipsilateral and contralateral tumors treated with dual and combo therapies (Fig. 3c; Fig. 6c), indicating an increase in antigen-specific, polyfunctional effector T cells. QH-II-066 has a significant effect on the numbers and frequency of IFN-γ and IFN-γ/TNF-α producing CD8+ T cells on contralateral tumors treated with radiation (5 or 10 Gy). The analysis of splenic CD8 T cells indicated that due to lack of antigen, the CD8 T cells develop memory phenotype and show enhanced IFN-γ and TNF-α production (Fig. E16).

Together, these results indicate that QH-II-066 has direct anti-tumor activity, while a dual or triple combination with QH-II-066 may synergize with ipsilateral and abscopal anti-tumor activity mediated by increase in antigen-specific effector CD8+ T cells.

Discussion

We show that melanoma lines express $GABA_AR$s whose activity is activated by its ligand/agonist GABA and enhanced by specific benzodiazepines. This is consistent with the $GABA_AR$ forming a hetero-pentameric structure with a canonical αβαβγ subunit stoichiometry. We show that benzodiazepine QH-II-066 is capable of directly impairing melanoma cell viability, while reducing tumor volume in a syngeneic melanoma model, even at a benzodiazepine dose comparable to that administered for adult patients for a wide range of clinical conditions, including anxiety. We also find that QH-II-066 potentiates radiation, even at a sub-optimal dose, and α-PD-L1 to enhance both ipsilateral and distant abscopal anti-tumor responses. The response is associated with enhanced tumor infiltration of CD8+ T cells that produce IFN-γ and TNF-α. There is also enhanced expression of genes with roles in cytokine:cytokine receptor activity, transcription factors in the p53 pathway (notably p63), and genes concordant with microRNA mir-17 overexpression.

In a ‘direct’ contribution to tumor control, benzodiazepine appears to enhance membrane anion permeability in tumor cells, which depolarizes their mitochondria, as we observe in cell culture experiments, and thereby elicits an apoptotic response. As noted, perturbation in ion homeostasis may also underly the enhanced expression of genes involved in p53 pathway signaling and cytokine:cytokine receptor activity and signaling, which we find in the treated tumors. In particular, we find enhanced expression of p63 target genes in all treatment groups in comparison to the control. Increased p63 expression after genotoxic treatment of melanoma cells has been observed and shown to interfere with p53 mediated apoptosis by the mechanism that involves mitochondrial translocation.[37] The increase of p63 expression was comparable in both radiation and combined QH-II-066 plus radiation treated samples, but it is plausible that depolarization of mitochondria by QH-II-066 interferes with the anti-apoptotic function of the p63 protein. Interestingly, breast cancer tumors exhibit enriched IFN-γ signaling that is associated with enhanced p63 expression[40], highlighting an important connection between p63 and immune signaling. Further, p63 has been reported to suppress both tumorigenesis and metastatic spread in a murine model by mediating down-regulation of the microRNA processing enzyme Dicer as well as the ‘oncomiRNA’ miR-130b.[41] Our observation that there is enhanced expression of genes associated with overexpression of the microRNA mir-17 is intriguing, as *MIR17* expression has also been shown to be enhanced by p63.[38] It may be that p63 enhanced expression in melanoma cells regresses the tumors in part by controlling Dicer and miRNA activity.

In an ‘indirect’ mechanism to tumor control, benzodiazepine QH-II-066 may enhance CD8+ T cell infiltrate into the melanoma tumor milieu to contribute to potentiating the response to radiation and immune checkpoint inhibition. As noted, QH-II-066 has a small effect on cell viability *in vitro*, as assessed by its micromolar IC_{50}, while *in vivo* when administered in combination with radiation and/or an immune checkpoint inhibitor, or even on its own at a higher dose, regresses the tumors. Perhaps QH-II-066 is modulating $GABA_AR$ receptors on CD8+ T cells.[42] Indeed, $GABA_AR$s have been reported to be expressed in CD8+ T cells (as well as in neutrophils, monocytes, CD3+ and CD4+ T cells) and GABAergic signaling has been observed to contribute to responses to intracellular pathogens[43] and autoimmune diseases.[44]

Future experimental effort will need to address whether QH-II-066 acts in synergy with radiation and/or immune checkpoint inhibitor or if its effect is additive. In addition, it remains open how QH-II-066 potentiates radiation, whether its potentiation of radiation is the same as how it might potentiate immune checkpoint inhibitor, and whether the effect of QH-II-066 is related to creating significant oxidative stress in the melanoma cells. The results of this study suggest that use of benzodiazepine to modulate $GABA_AR$ as a 'sensitizer' of melanoma tumors to radiation and/or an immune checkpoint inhibitor is a future avenue to explore clinically. Repurposing of a benzodiazepine in such therapeutic combinations has the potential to improve outcomes for patients in a rapidly translatable and cost-effective manner.[45]

Supplementary Material

Refer to Web version on PubMed Central for supplementary material.

References

1. Shonka N, Venur VA, Ahluwalia MS. Targeted treatment of brain metastases. Curr Neurol Neurosci Rep 2017;17:37. [PubMed: 28326470]
2. Davies H, et al. Mutations of the BRAF gene in human cancer. Nature 2002;417:949–954. [PubMed: 12068308]
3. Hodis E, et al. A landscape of driver mutations in melanoma. Cell 2012;150:251–263. [PubMed: 22817889]
4. McArthur GA, et al. Vemurafenib in metastatic melanoma patients with brain metastases: an open-label, single-arm, phase 2, multicentre study. Ann Oncol 2017;28: 634–641. [PubMed: 27993793]
5. Falchook GS, et al. Dabrafenib in patients with melanoma, untreated brain metastases, and other solid tumours: a phase 1 dose-escalation trial. Lancet 2012;379:1893–1901. [PubMed: 22608338]
6. Long GV, et al. Dabrafenib in patients with Val600Glu or Val600Lys BRAF-mutant melanoma metastatic to the brain (BREAK-MB): a multicentre, open-label, phase 2 trial. Lancet Oncol 2012;13:1087–1095. [PubMed: 23051966]
7. Davies MA, et al. Dabrafenib plus trametinib in patients with BRAF(V600)-mutant melanoma brain metastases (COMBI-MB): a multicentre, multicohort, open-label, phase 2 trial. Lancet Oncol 2017;18:863–873. [PubMed: 28592387]
8. Hauschild A, et al. Dabrafenib in BRAF-mutated metastatic melanoma: a multicentre, open-label, phase 3 randomised controlled trial. Lancet 2012;380:358–365. [PubMed: 22735384]
9. Sosman JA, et al. Survival in BRAF V600-mutant advanced melanoma treated with vemurafenib. N Engl J Med 2012;366:707–714. [PubMed: 22356324]
10. Turajlic S, et al. Whole-genome sequencing reveals complex mechanisms of intrinsic resistance to BRAF inhibition. Ann Oncol 2014;25:959–967. [PubMed: 24504448]
11. Tirosh I, et al. Dissecting the multicellular ecosystem of metastatic melanoma by single-cell RNA-seq. Science 2016;352:189–196. [PubMed: 27124452]
12. Tawbi HA, et al. New era in the management of melanoma brain metastases. Am. Soc. Clin Oncol Educ Book 2018;38:741–750. [PubMed: 30231345]
13. Tawbi HA, et al. Combined nivolumab and ipilimumab in melanoma metastatic to the brain. N Engl J Med 2018;379:722–730. [PubMed: 30134131]
14. Postow MA, Sidlow R, Hellmann MD. Immune-related adverse events associated with immune checkpoint blockade. N Engl J Med 2018;378:158–168. [PubMed: 29320654]
15. Wolchok JD, et al. Overall survival with combined nivolumab and ipilimumab in advanced melanoma. N Engl J Med 2017;377:1345–1356. [PubMed: 28889792]
16. Larkin J, Hodi FS, Wolchok JD. Combined nivolumab and ipilimumab or monotherapy in untreated melanoma. N Engl J Med 2015;373:1270–1271.

17. Akbani R, et al. Genomic classification of cutaneous melanoma. Cell 2015;161:1681–1696. [PubMed: 26091043]
18. Kallay L, et al. Modulating native GABAA receptors in cancer cells with positive allosteric benzodiazepine-derivatives induces cell death. J Neuro-Oncol 2019;142:411–422.
19. Cook JM, et al. Stereospecific anxiolytic and anticonvulsant agents with reduced muscle-relaxant, sedative-hypnotic and ataxic effects. US Patent 7119196 B2. 2006.
20. Dobin A, Davis CA, Schlesinger F, Drenkow J, Zaleski C, Jha S. STAR: ultrafast universal RNA-seq aligner. Bioinformatics 2013;29:15–21. [PubMed: 23104886]
21. Liao Y, Smyth GK, Shi W. FeatureCounts: an efficient general purpose program for assigning sequence reads to genomic features. Bioinformatics 2013;30:923–930. [PubMed: 24227677]
22. Anders S, McCarthy DJ, Chen Y, Okoniewski M, Smyth GK, Huber W, Robinson MD. Count-based differential expression analysis of RNA sequencing data using R and Bioconductor. Nat Protocols 2013;8:1765–1786. [PubMed: 23975260]
23. Benjamini Y, Hochberg Y. Controlling the false discovery rate: a practical and powerful approach to multiple testing. J Royal Stat Soc B 1995;57:289–300.
24. Kanehisa M, Furumichi M, Tanabe M, Sato Y, Morishima K. KEGG: new perspectives on genomes, pathways, diseases and drugs. Nucleic Acids Res 2017;45: D353–D361. [PubMed: 27899662]
25. Garcia-Alonso L, Holland CH, Ibrahim MM, Turei D, Saez-Rodriguez J. Benchmark and integration of resources for the estimation of human transcription factor activities. Genome Res 2019;29:1363–1375. [PubMed: 31340985]
26. Godec J, Tan Y, Liberzon A, Tamayo P, Bhattacharya S, Butte AT, Mesirov JP, Haining WN. Compendium of immune signatures identifies conserved and species-specific biology in response to inflammation. Immunity 2016;44:194–206. [PubMed: 26795250]
27. Subramanian A, et al. Gene set enrichment analysis: a knowledge-based approach for interpreting genome-wide expression profiles. Proc Natl Acad Sci USA 2005;102:15545–15550. [PubMed: 16199517]
28. Korotkevich G, Sukhov V, Sergushichev A. Fast gene set enrichment analysis. bioRxiv 2019;060012.
29. Gu Z, Eils R, Schlesner M. Complex heatmaps reveal patterns and correlations in multidimensional genomic data. Bioinformatics 2016;32:2847–2849. [PubMed: 27207943]
30. Sigel E, Steinmann ME. Structure, function, and modulation of GABAA receptors. J Biol Chem 2012;287:40224–40231. [PubMed: 23038269]
31. Sieghart W. Allosteric modulation of GABAA receptors via multiple drug-binding sites. Adv Pharmacol 2015;72:53–96. [PubMed: 25600367]
32. Clayton T, et al. An updated unified pharmacophore model of the benzodiazepine binding site on gamma-aminobutyric acid(a) receptors: correlation with comparative models. Curr Med Chem 2007;14:2755–2775. [PubMed: 18045122]
33. Clayton T, et al. A review of the updated pharmacophore for the alpha 5 gaba(a) benzodiazepine receptor model. Int J Med Chem 2015;2015:430248.
34. Sengupta S, et al. a5-GABAA receptors negatively regulate MYC-amplified medulloblastoma growth. Acta Neuropathol 2014;127:593–603. [PubMed: 24196163]
35. Jonas O, et al. First in vivo testing of compounds targeting Group 3 medulloblastomas using an implantable microdevice as a new paradigm for drug development. J Biomed Nanotech 2016;12:1297–302.
36. Platt DM, et al. Contribution of alpha 1GABAA and alpha 5GABAA receptor subtypes to the discriminative stimulus effects of ethanol in squirrel monkeys. J Pharmacol Exp Ther 2005;313:658–667. [PubMed: 15650112]
37. Matin RN, et al. p63 is an alternative p53 repressor in melanoma that confers chemoresistance and a poor prognosis. J Exp Med 2013;210:581–603. [PubMed: 23420876]
38. Ratovitski EA. Tumor protein p63/microRNA network in epithelial cancer cells. Current Genomics 2013;14:441–452. [PubMed: 24396276]

39. Wang C, Youle RJ. The role of mitochondria in apoptosis. Annu Rev Genet 2009;43:95–118. [PubMed: 19659442]
40. Mehta SY. Regulation of the interferon-gamma (IFN-γ) pathway by p63 and Δ133p53 isoform in different breast cancer subtypes. Oncotarget 2018;9:29146–29161. [PubMed: 30018742]
41. Su X, et al. TAp63 suppresses metastasis through coordinate regulation of Dicer and miRNAs. Nature 2010;467:986–990. [PubMed: 20962848]
42. Mendu SK, et al. Different subtypes of GABA-A receptors are expressed in human, mouse and rat T lymphocytes. PLoS One 2012;7:e42959.
43. Kim JK, et al. GABAergic signaling linked to autophagy enhances host protection against intracellular bacterial infections. Nat Commun 2018;9:4184. [PubMed: 30305619]
44. Jin Z, Mendu SK, Birnir B. GABA is an effective immunomodulatory molecule. Amino Acids 2013;45:87–94. [PubMed: 22160261]
45. Khan MK, et al. Repurposing drugs for cancer radiotherapy: early successes and emerging opportunities. Cancer J 2019;25:106–115. [PubMed: 30896532]
46. Friedman H, et al. Pharmacokinetics and pharmacodynamics of oral diazepam: effect of dose, plasma concentration, and time. Clin Pharmacol Ther 1992;52:139–150. [PubMed: 1505149]
47. Berro LF, et al. GABAa receptor subtypes and the abuse-related effects of ethanol in rhesus monkeys: experiments with selective positive allosteric modulators. Alcohol Clin Exp Res 2019;43:791–802. [PubMed: 30861153]
48. Kanehisa M, Furumichi M, Tanabe M, Sato Y, Morishima K. KEGG: new perspectives on genomes, pathways, diseases and drugs. Nucleic Acids Res 2017;45:D353–D361. [PubMed: 27899662]
49. Su AI, Wiltshire T, Batalov S, Lapp H, Ching KA, Block D, Zhang J, Soden R, Hayakawa M, Kreiman G, Cooke MP, Walker JR, Hogenesch JB. A gene atlas of the mouse and human protein-encoding transcriptomes. Proc Natl Acad Sci USA 2004;101:6062–6067. [PubMed: 15075390]
50. Robinson MD, McCarthy DJ, Smyth GK. edgeR: a Bioconductor package for differential expression analysis of digital gene expression data. Bioinformatics 2010;26: 139–140. [PubMed: 19910308]

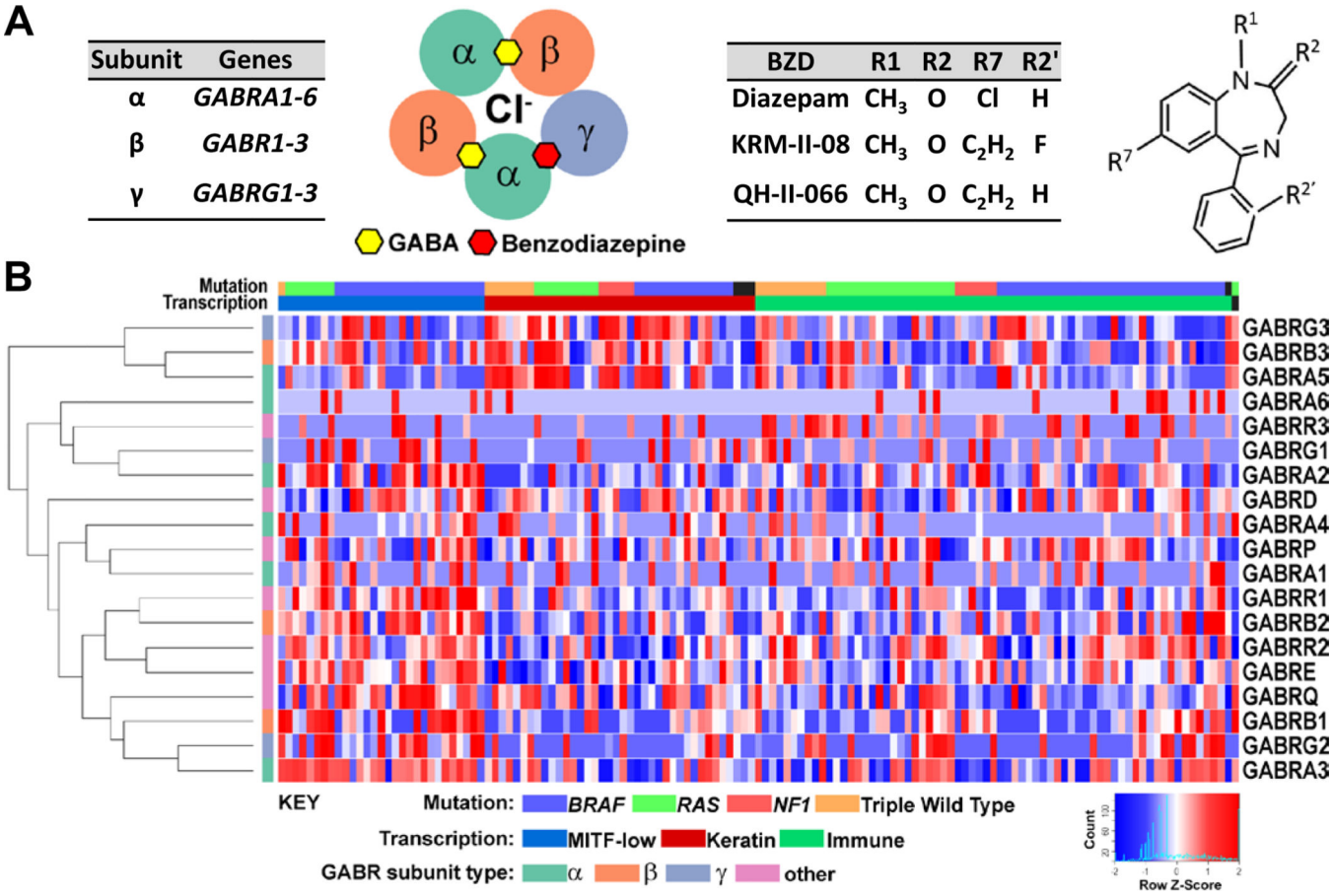

Figure 1. GABA$_A$ receptor expression in metastatic melanoma.

(**A**) Type-A GABA receptors (GABA$_A$Rs) are composed most commonly of two α, two β, and γ subunits encoded by *GABR* genes *GABRA (1–6)*, *GABRB (1–3)*, and *GABRG (1-3)*, respectively. GABA$_A$R consists of five subunit transmembrane segments which create the chloride (Cl^-) conduction pore. Inter-subunit binding sites for GABA (yellow hexagon) and benzodiazepine (red hexagon) are shown, recognizing the αβαβγ subunit stoichiometry. Benzodiazepines have a common core structure. Shown are sites frequently modified (R1, R2, R2′, R7), which may impart a GABA$_A$R subtype-preference. GABA$_A$R subtype-preferring benzodiazepines (BZDs) KRM-II-08 and QH-II-066 differ from diazepam by having an R7 acetylene group. (**B**) Normalized expression data for *GABR* genes from stage III/IV melanoma specimens. Samples were classified into three melanoma molecular subgroups. Heatmap for analysis of expression across subgroups was generated using Morpheus (https://software.broadinstitute.org/morpheus).

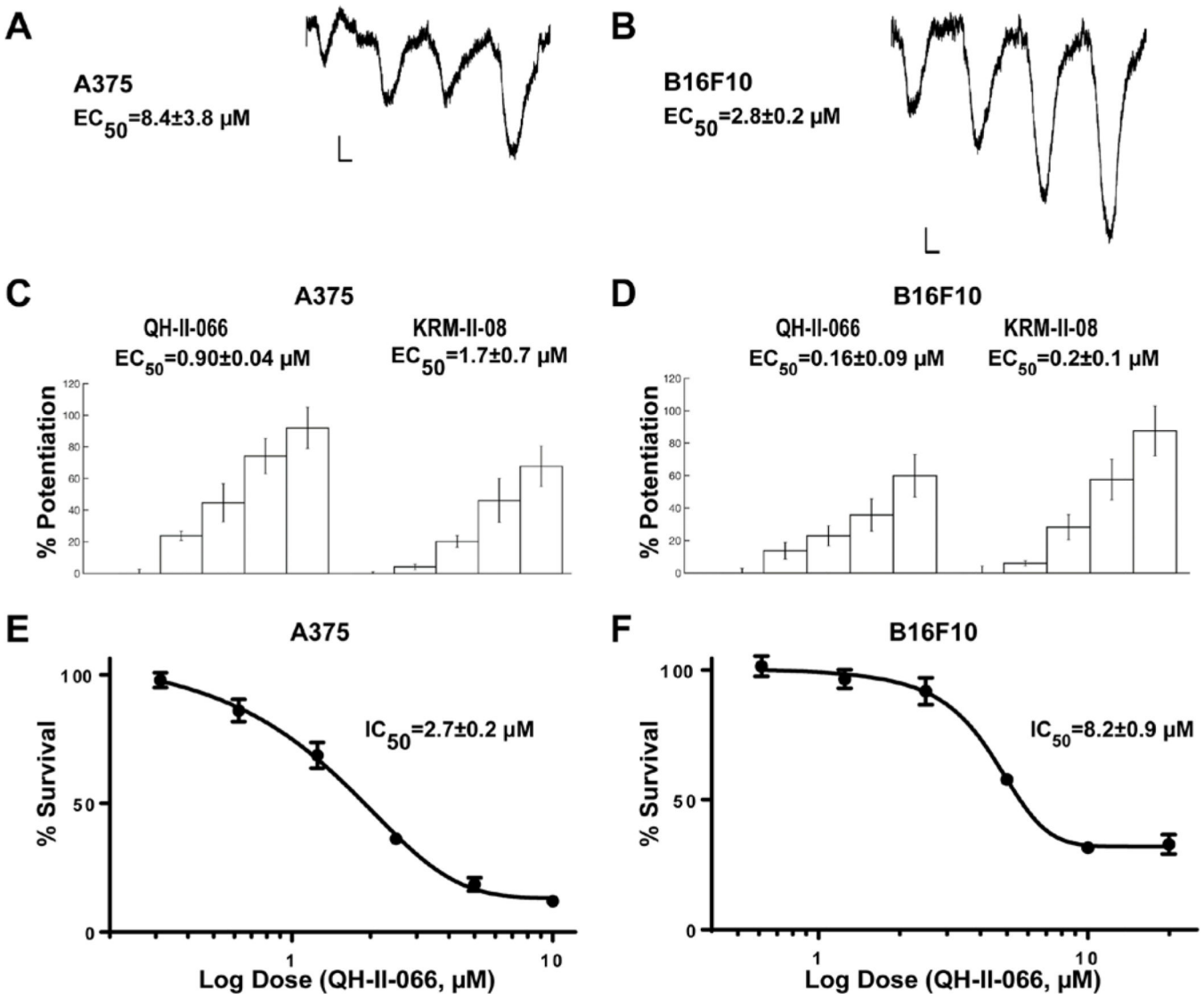

Figure 2. Characterization of melanoma $GABA_A$ receptors.

Representative electrophysiology recordings of transmembrane anion flow in human melanoma line A375 (**A**) and mouse melanoma line B16F10-GP (**B**) in response to GABA (1, 3, 10, 30 μM). Horizontal calibration bars, 2 seconds; vertical bars, 500 pA; sweeps are ensemble recordings from 8 electrodes. Potentiation of GABA responses in A375 (**C**) and B16F10-GP (**D**) cells in response to benzodiazepines (QH-II-066 and KRM-II-08 at 0, 0.3, 1, 3, 10 μM). GABA concentration was 1 μM. *In vitro* MTS assay of A375 (**E**) and B16F10-GP (**F**) cells in response to QH-II-066.

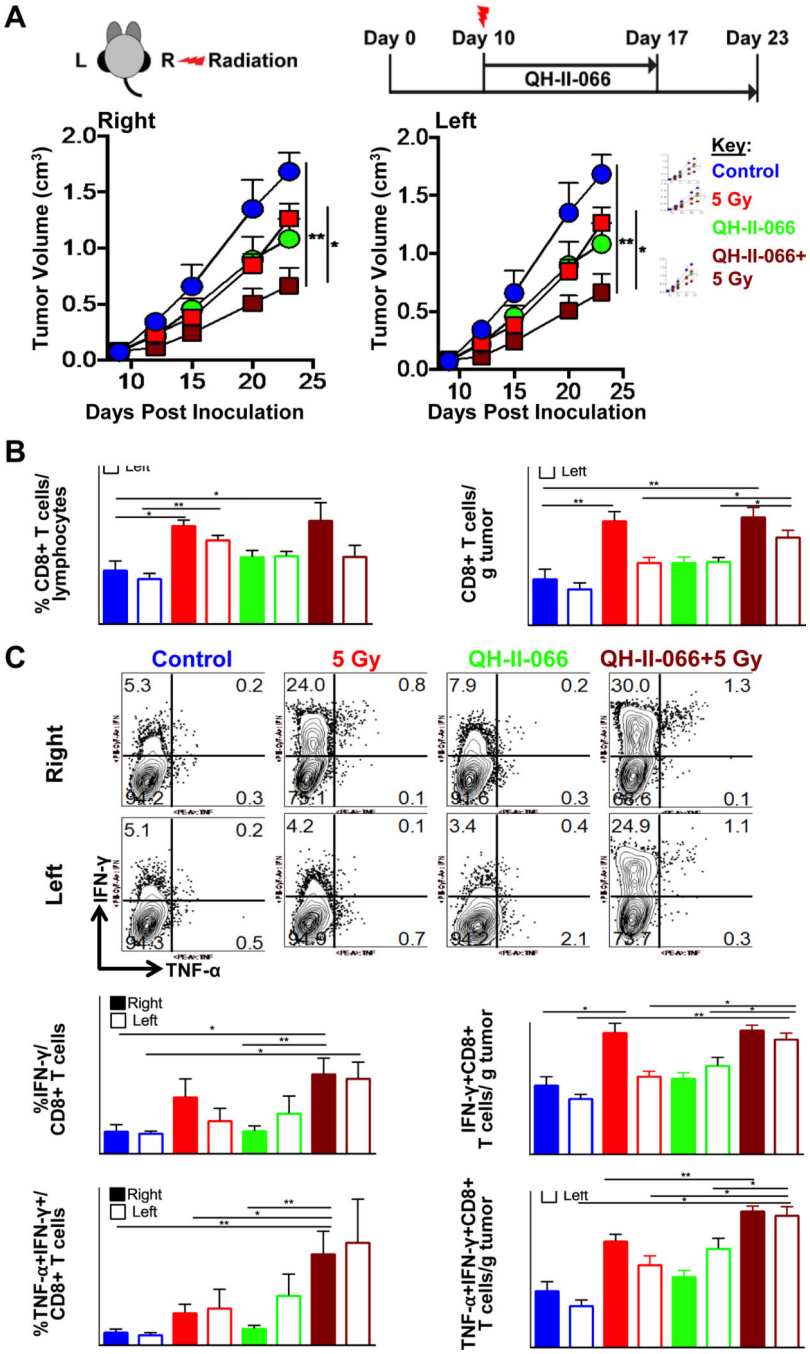

Figure 3. Benzodiazepine potentiates radiation.

(**A**) **Top**, Schematic showing therapeutic strategy. Mice were implanted in left (L) and right (R) flanks with B16F10-GP tumor cells. Mice received either: (*i*) vehicle alone control; (*ii*) radiation alone (5 Gy, right-flank only); (*iii*) QH-II-066 beginning Day 10; (*iv*) radiation (5 Gy, right-flank only) on Day 10 (morning), followed by QH-II-066 (evening). **Bottom**, Effect of combination of QH-II-066 and 5 Gy on tumor growth kinetics. Tumor measurements are combination of two experiments; where, vehicle alone control, n=8; 5 Gy, n=9; QH-II-066, n=8; QH-II-066+5 Gy, n=9. In groups receiving QH-II-066, 10 mg/kg was

injected i.p. daily for 7 days. (**B**) Percent CD8 of total lymphocytes and number of CD8 T cells per gram of tumor. TILs were isolated at day 7–8 after radiation. Error bars are representation of SEM. (**C**) **Top**, Representative flow showing percent IFN-γ and TNF-α in total CD8+ T cells after TILs were stimulated with peptide. **Middle**, Graph showing percent IFN-γ+CD8+ of total CD8+ T cells and number of IFN-γ+CD8 T+ cells per gram of tumor. **Bottom**, Graph showing percent TNF-α +CD8+ of total CD8+ T cells and number of TNF-α +CD8 T+ cells per gram of tumor. (*p<0.05; **p<0.01; ***p<0.001; ****p<0.0001). *Abbreviation*: i.p., intraperitoneal; TILs, Tumor infiltrating lymphocytes; IFN-γ, interferon gamma cytokine; TNF-α, Tumor necrosis factor alpha cytokine.

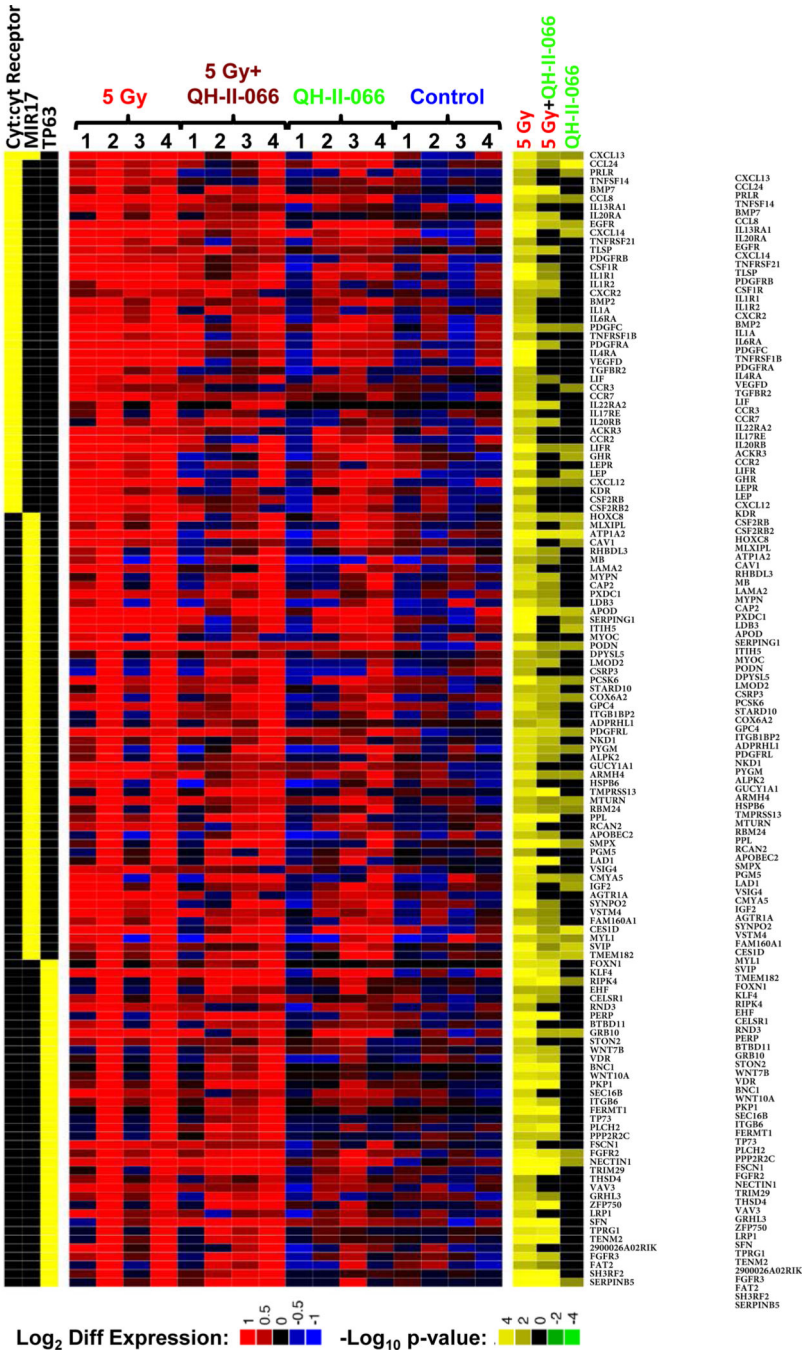

Figure 4. Differential gene expression in treated mouse tumors.

Expression levels of differentially expressed genes in enriched immunity-related KEGG pathway (cyt:cyt Receptor is abbreviation for cytokine:cytokine receptor), p63 target genes, and enhanced expression of genes associated with overexpression of microRNA mir-17, identified by enrichment analysis of the ImmuneSigDB compendium of transcriptional immune signatures.[26, 48, 49] Genes in the enriched gene sets were considered to be differentially expressed if edgeR FDR<0.05 in any one of the 3 comparisons. **Left**, heatmap indicates membership of each gene (rows) in the enriched gene sets (columns). **Middle**,

heatmap displays expression levels of genes in individual samples (columns) in terms of log2 counts per million (LCPM).[50] Each LCPM has been normalized by subtracting the gene-specific average LCPM of the untreated samples. **Right**, heatmap displays statistical significance and the direction of the change in each of the comparisons made (5 Gy vs Control; 5 Gy+QH-II-066 vs Control; QH-II-066 vs Control) (columns), each vs control. The statistical significance is expressed in log10(p-value) when expression ratio was less than 1 (down-regulation) and -log10(p-value) when expression ratio was greater than 1 (up-regulation) resulting in negative numbers for downregulation and positive for upregulation. *Abbreviation*: FDR, false discovery rate.

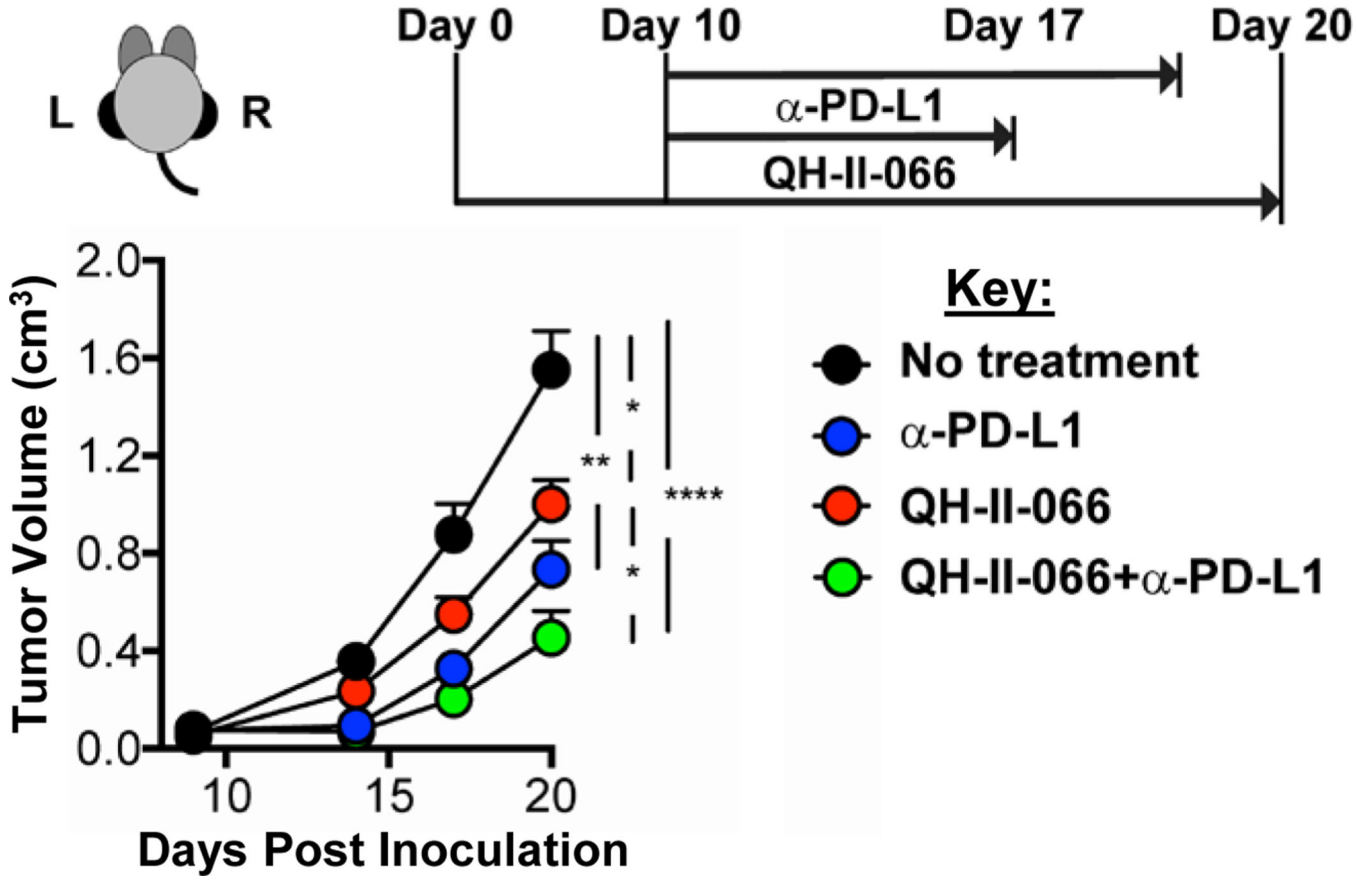

Figure 5. Benzodiazepine potentiates immune checkpoint inhibitor.

Top, Schematic showing therapeutic strategy. Mice were implanted in left (L) and right (R) flanks with B16F10-GP cells (Day 0). Day 10, mice received either: (*i*) vehicle alone control; (*ii*) QH-II-066; (*iii*) α-PD-L1; (*iv*) QH-II-066+α-PD-L1. **Bottom,** Effect of combination of QH-II-066 and α-PD-L1 on tumor growth kinetics. In groups receiving QH-II-066, 10 mg/kg was injected i.p. daily for 7 days. In group receiving α-PD-L1, 200 μg was injected i.p. every 3 days through end of the experiment. Tumor measurements were taken with 7–8 mice per group with a tumor on each flank; where, vehicle alone control, n=7; α-PD-L1, n=8; QH-II-066, n=7; QH-II-066+ α-PD-L1, n=7. (*p<0.05; **p<0.01; ***p<0.001; ****p<0.0001). *Abbreviation*: PD-L1 = programmed death-ligand 1; i.p., intraperitoneal.

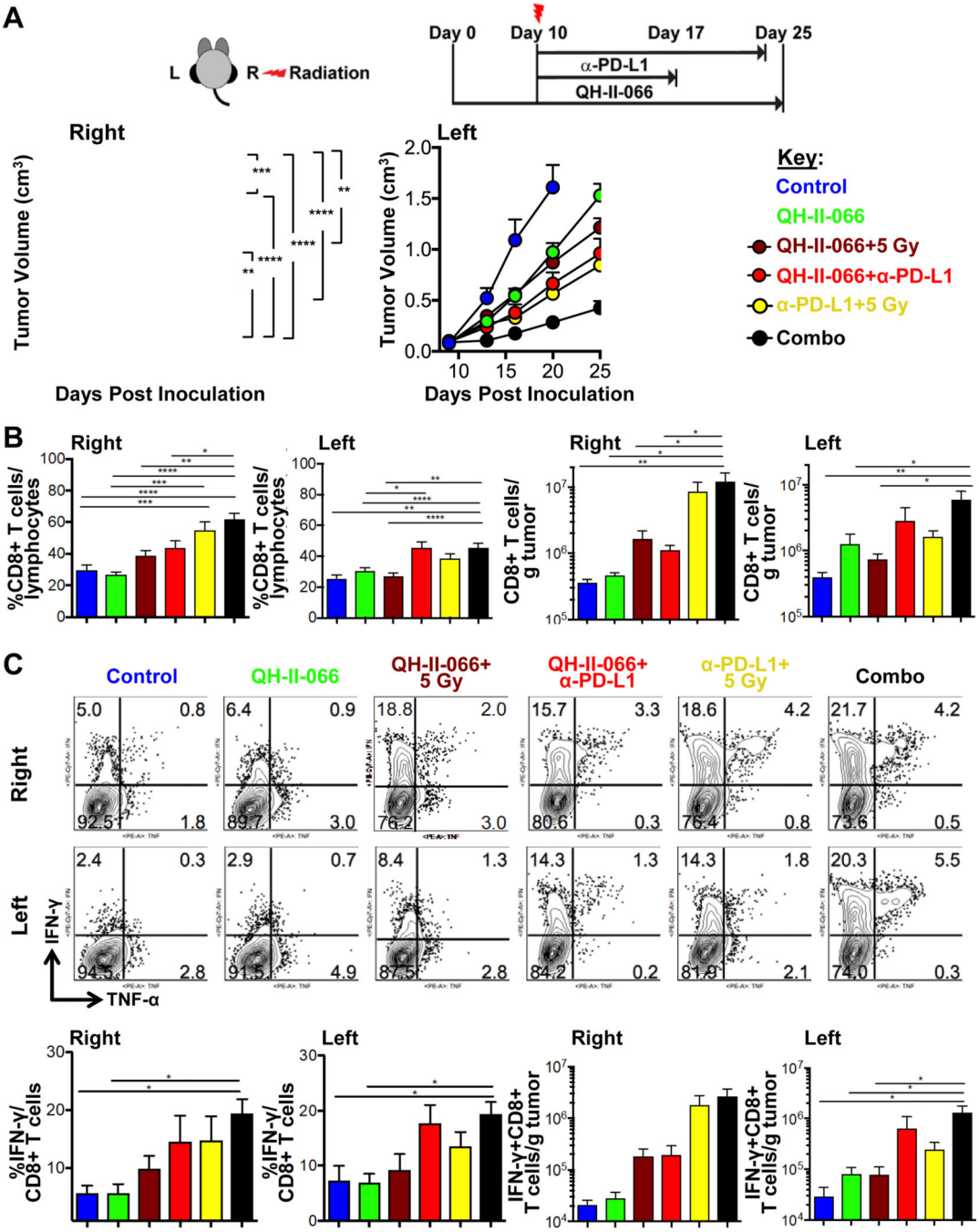

Figure 6. Effectiveness of polytherapy.

(**A**) **Top**, Schematic showing the therapeutic strategy. Mice were implanted in left (L) and right (R) flanks with B16F10-GP cells (Day 0). Day 10, mice received either: (*i*) vehicle alone control; (*ii*) QH-II-066; (*iii*) radiation (5 Gy, right-flank only) on Day 10 (morning), followed by QH-II-066 (evening); (*iv*) QH-II-066+α-PD-L1, beginning on day 10; radiation (5 Gy, right-flank only) on Day 10 (morning), followed by α-PD-L1 (in the evening). In groups receiving QH-II-066, 10 mg/kg was injected i.p. daily for 7 days. In group receiving α-PD-L1, 200 μg was injected i.p. every 3 days through the end of experiment or maximum

5 injections. **Bottom,** Effect of combination of dual and triple therapy on tumor growth kinetics. Tumor measurements were taken with 10 mice per each group. For kinetics of tumor volume, tumors were measured at Indicated time points and experiment was done twice. The data is combination of both experiments. (*p<0.05; **p<0.01; ***p<0.001; ****p<0.0001). (**B**) Percent CD8 of total lymphocytes and number of CD8 T cells per gram of tumor in right and left tumors. TILs were isolated at day 7–8 after radiation and stained with indicated antibodies. Error bars are representation of SEM. (**C**) **Top and Middle,** Representative flow showing percent IFN-γ and TNF-α in total CD8+ T cells after TILs were stimulated with peptide, as described in materials and methods. IFN-γ and TNF-α were stained with appropriate antibodies by intracellular staining. **Bottom,** Graph summarizing the percent IFN-γ+CD8+ of total CD8+ T cells and number of IFN-γ+CD8 T + cells per gram of tumor. *Abbreviation*: PD-L1 = programmed death-ligand 1; TILs, Tumor infiltrating lymphocytes; IFN-γ, interferon gamma cytokine; TNF-α, Tumor necrosis factor alpha cytokine.